Optimizing steady-state synchronization in disordered semiconductor lasers

Li-Li Ye,[1] Nathan Vigne,[2] Fan-Yi Lin,[2,3] Hui Cao,[2,*] and Ying-Cheng Lai[1,4,†]

[1] *School of Electrical, Computer and Energy Engineering, Arizona State University, Tempe, Arizona 85287, USA*

[2] *Department of Applied Physics, Yale University, New Haven, Connecticut 06520, USA*

[3] *Institute of Photonics Technologies, Department of Electrical Engineering, National Tsing Hua University, Hsinchu 30013, Taiwan*

[4] *Department of Physics, Arizona State University, Tempe, Arizona 85287, USA*

(Dated: December 3, 2025)

Disorder can profoundly influence synchronization in networks of nonlinear oscillators, sometimes enhancing coherence through external tuning. In semiconductor lasers, however, achieving high-quality steady-state synchronization is desired, while intrinsic and typically uncontrollable disorder poses a major challenge. Under fixed frequency disorder, we investigate homogeneous fully coupled external-cavity semiconductor lasers governed by the complex, time-delayed Lang-Kobayashi equations with experimentally relevant parameters and identify an optimal coupling strength that maximizes steady-state synchronization in the weak-coupling regime. This optimum appears for any fixed configuration of intrinsic frequency detuning and scales inversely with the number of lasers, leading to a linear scaling of the total coupling cost with the number of lasers. A theory based on an effective thermodynamic potential explains this disorder-mediated optimization, revealing a general mechanism by which moderate coupling can overcome static heterogeneity in nonlinear physical systems.

Synchronization in complex dynamical systems has been a topic of continuous interest [1, 2]. A common setting is coupled dynamical oscillators, where the bifurcation parameter is the coupling strength among the oscillators. A focus of many previous studies was on identifying the critical point at which a transition from desynchronization to synchronization occurs. Depending on the dynamics of the oscillators and the coupling function, the system can have a sequence of transitions, giving rise to characteristically distinct synchronization behaviors in the parameter space. For example, for a system of coupled identical nonlinear oscillators, complete synchronization can arise when the coupling exceeds a critical strength as determined by the master stability function [3, 4]. In networks of identical chaotic oscillators (without spatial disorder), synchronization can be made most stable by appropriately tuning the coupling strength [5], an effect reminiscent of a resonance and well described by the master-stability-function framework. Our problem, however, is fundamentally different: we aim to optimize steady-state synchronization in coupled semiconductor lasers with strong intrinsic disorder, a regime in which the master-stability theory no longer applies. Systems of phase oscillators with nonlinear coupling, e.g., those described by the classic Kuramoto model [1], can host phase synchronization and the critical coupling strength required for the onset of this type of "weak" synchronization can be determined by the mean-field theory [6, 7]. A recent study [8] employed a gradient-based optimization approach to identify an optimal sparse coupling structure that maximizes synchrony in the disordered Kuramoto model. Synchronization in coupled oscillators was experimentally studied [9, 10]. A counterintuitive phenomenon is that adding connections can hinder network synchronization of time-delayed oscillators [11]. Biomedical applications of synchronization have also been actively studied [12].

There is a large body of literature on synchronization in networks of nonlinear oscillators [13, 14]. A remarkable phenomenon is that disorders, e.g., random parameter heterogeneity among the oscillators, can counterintuitively maximize [15] and promote [16, 17] synchronization. For coupled chaotic oscillators, parameter regimes can arise where the oscillator heterogeneity leads to synchronization for conditions under which identical oscillators cannot be synchronized [18]. Synchronization in networked systems with large parameter mismatches was studied in terms of the stability of the synchronous state and transition [19]. Of physical significance with considerable theoretical and experimental interests are external-cavity semiconductor lasers [20–31], mathematically described by the time-delayed nonlinear Lang–Kobayashi (LK) equations [32]. Previous studies of evanescently coupled semiconductor laser arrays [28, 33] demonstrated that phase-locked states are readily destabilized above threshold, with the onset of instability depending critically on the ratio of carrier to photon lifetimes. For an array of fully coupled external cavity semiconductor lasers with spatially decaying coupling, two recent theoretical studies [22, 34] proposed achieving and enhancing synchronization by exploiting disorder. Specifically, Ref. [22] demonstrated that synchronization can be promoted when time-delay-induced disorder compensates for intrinsic frequency disorder, while Ref. [34] showed that frequency synchronization can be stabilized by introducing intermediate random mismatches among

* hui.cao@yale.edu

† Ying-Cheng.Lai@asu.edu

otherwise identical lasers, including frequency, coupling, and amplitude-phase coupling disorders. In both studies, the disorders were treated as tunable parameters. While it is possible to experimentally tune the frequency disorder of semiconductor lasers by changing either electrical current or optical pump power for individual lasers, this requires precise control that may be experimentally challenging.

Frequency disorder in semiconductor laser networks [8, 22, 34, 35] is unavoidable, primarily arising from manufacturing imperfections [36, 37]. Such disorder disrupts synchronization and limits the achievable coherence and output power. Although chaotic dynamics in semiconductor lasers have been successfully exploited for applications such as secure communication [38, 39], random number generation [40], and LiDAR/radar systems [41–43], they can be detrimental in experiments and systems that require coherent, high-power output. In such contexts, stable steady-state synchronization is the preferred operating regime. Recent advances in optical control have enabled the engineering of coupling topologies [44], for example, all-to-all coupling implemented via a spatial light modulator (SLM), as shown in Fig. 1, which can also be realized without an SLM [45–47]. In practice, however, the total coupling strength, which reflects the experimental coupling cost, is often constrained. This raises a fundamental question: for a given configuration of frequency disorder and within the weak-coupling regime, can one identify an optimal coupling strength that maximizes steady-state synchronization across the entire network?

This Letter provides an affirmative answer. We demonstrate that, for fixed frequency disorder, the coupling strength in a homogeneous, all-to-all coupled laser network can be tuned to achieve high-quality steady-state synchronization. In the weak-coupling regime, the global coupling strength is much smaller than the statistical spread (standard deviation) of the frequency disorder. Qualitatively, steady-state synchronization arises from the intricate interplay among frequency disorder, coupling effects, and dynamical stability in the optical fields. In the absence of coupling, the free-running lasers remain in steady states with different intrinsic frequencies, and this frequency disorder prevents synchronization. Increasing the global coupling strength within the weak-coupling regime can gradually pull all different frequencies toward the same final dynamical frequency but eventually drives the system toward chaotic dynamics, which are undesirable, as shown in Fig. 2. Consequently, as the coupling strength increases, steady-state synchronization reaches its maximum just before the onset of chaos, representing a trade-off among disorder, coupling, and stability. A remarkable finding is that, the optimal coupling strength for maximizing steady-state synchronization scales inversely with the network size, making it possible to synchronize a large number of semiconductor lasers in the weak coupling regime. This leads to a linear scaling of the total coupling cost with the number M of lasers, which is much more desirable than the M^2 scaling if the critical coupling coefficient were independent of M.

To explain our findings, we develop a theoretical framework that recasts the delayed phase dynamics as a gradient flow on an effective thermodynamic potential, where steady-state solutions correspond to local minima of the potential. This framework elucidates the observed scaling of the optimal coupling with system size. Although it has been qualitatively recognized in the laser community that coupling must be neither too weak nor too strong to achieve synchronization, a systematic study and quantitative understanding in semiconductor laser networks have been lacking until now.

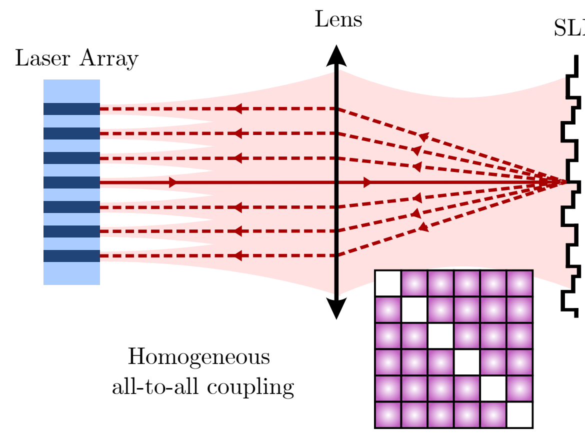

FIG. 1. Illustration of a network of coupled semiconductor diode lasers. Experimentally, coupling is implemented using a spatial light modulator (SLM) placed at the back focal plane of a collimation lens, with the laser array located at the front focal plane. Lasers at different transverse positions are coupled through gratings of corresponding periods on the SLM, introducing a delay determined by the round-trip time τ between the array and the SLM. The intrinsic lasing frequencies of the individual lasers are randomly detuned due to unavoidable fabrication-induced heterogeneity.

A network of M coupled diode lasers, each operating in a single longitudinal and transverse mode at fixed polarization with frequency disorders, is described by the LK equations [22, 32]:

$$\frac{dE_i(t)}{dt} = \frac{1+i\alpha}{2}\left(g\frac{N_i(t)-N_0}{1+s|E_i(t)|^2}-\gamma\right)E_i(t) + i\Delta_i E_i(t) + e^{-i\omega_0\tau}\kappa\sum_{j\neq i}E_j(t-\tau),$$

$$\frac{dN_i(t)}{dt} = J_0 - \gamma_n N_i(t) - g\frac{N_i(t)-N_0}{1+s|E_i(t)|^2}|E_i(t)|^2, \quad (1)$$

where $E_i(t)$ is the complex electric field of the ith laser, $N_i(t)$ is the carrier number governed by the pump rate $J_0 = 4J_{th}$ with $J_{th} = \gamma_n(N_0+\gamma/g)$ being the single-laser pump rate at threshold, γ_n is the carrier loss rate, N_0 is the carrier number at transparency, γ is the cavity loss rate, g is the differential gain coefficient, and τ is the time delay due to the external cavity. The typical experimental parameter values are $\gamma_n = 0.5\,\mathrm{ns}^{-1}$, $N_0 = 1.5 \times 10^8$, $\gamma = 500\,\mathrm{ns}^{-1}$, and $g = 1.5 \times 10^{-5}\,\mathrm{ns}^{-1}$. Other experimental parameter values are: the amplitude–phase coupling (linewidth enhancement) factor $\alpha = 5$, gain saturation coefficient $s = 2 \times 10^{-7}$, and external time delay $\tau = 3\,\mathrm{ns}$. Random frequency disorders are modeled as $\Delta_i = \sigma_\Delta \mathcal{N}(0,1)$, where $\mathcal{N}(0,1)$ is a Gaussian random variable with zero mean and unit variance. The natural angular frequency reference ω_0 is chosen such that $\omega_0 \tau = 2N\pi$ with N selected to be closest to the mean of all natural angular frequencies. The frequency disorder values are ordered as $\Delta_1 \le \Delta_2 \le \ldots \le \Delta_M$, with $\sigma_\Delta = 14\,\mathrm{rad/ns}$ and $M = 24$.

The laser field is expressed as $E_i(t) = r_i(t)e^{i\Omega_i(t)}$. Synchronization, encompassing the same amplitude, frequency, and phase, can be quantified by $\langle S \rangle = \langle |\sum_{i=1}^{M} E_i(t)|^2 / [M \sum_{i=1}^{M} |E_i(t)|^2] \rangle \in [0,1]$, where a larger value indicates stronger synchronization. If only frequency and phase synchronization are of interest, then $\langle S \rangle$ reduces to $\langle R^2 \rangle = \langle |\sum_{i=1}^{M} e^{i\Omega_i(t)}|^2 / M^2 \rangle$ since all lasers share the same amplitude $r_0(t)$. The Kuramoto model is a reduced phase-dynamics model derived from the LK equation, so $\langle R^2 \rangle$ is its standard choice. Because the LK equations include nonzero amplitude–phase coupling, it is preferable to use $\langle S \rangle$ so that amplitude synchronization is also taken into account. The all-to-all coupling configuration is described by $K_{ij} = \kappa(1 - \delta_{ij})$, with κ and δ_{ij} being the global coupling strength and Kronecker delta, respectively. The self-feedback coupling (the diagonal elements of the coupling matrix) is set to zero to avoid dynamical instabilities. Without frequency disorders, complete synchronization ($\langle S \rangle = 1$) occurs in both the weakly ($\kappa \ll \sigma_\Delta$) and strongly ($\kappa \gg \sigma_\Delta$) coupling regime.

When frequency disorder is present, optimized steady-state synchronization emerges in the weak-coupling regime ($\kappa \ll \sigma_\Delta$), with the optimal coupling $\kappa^* \in [0, 0.5]\,\mathrm{ns}^{-1}$ for $M \ge 24$. The synchronization measure attains $\langle S \rangle > 0.8$ (approaching unity) over the range $\sigma_\Delta \in [1, 14]\,\mathrm{rad/ns}$, independent of the number of lasers M, as shown in Figs. 2 and 3. For example, for $M = 24$ lasers, we have $\langle S \rangle_{\max} \approx 0.84$ for $\kappa^* \approx 0.4\,\mathrm{ns}^{-1}$, as shown in Fig. 2(a). Figures 2(b) and 2(c) display the fitted short-term frequencies and the fluctuations of the normalized intensities for $M = 24$, respectively. Our computations revealed that, in the presence of frequency disorders, the strong synchronization $\langle S \rangle > 0.8$ achieved in the weak coupling regime, is in fact steady-state synchronization, where the individual lasers maintain sinusoidal, nearly synchronous oscillations. This type of synchronization is desired in applications. In the strong-coupling regime ($\kappa \gg \sigma_\Delta$), chaotic dynamics emerge [22, 48, 49], but these are not relevant to steady-state synchronization.

Heuristically, the underlying mechanism for optimized steady-state synchronization, which occurs near the boundary between the steady-state and chaotic dynamical regimes in Fig. 2, can be described as follows. For $\kappa = 0$, the presence of frequency disorder prevents synchronization under steady-state dynamics. At small κ, the coupling is too weak to compensate for the frequency detuning, leading to only marginal improvement in synchronization. As κ increases, synchronization is progressively enhanced as long as the laser dynamics remain regular (non-chaotic). This trend ceases once irregular dynamics emerge, as shown in Figs. 2(b) and 2(c), resulting in a subsequent decrease in the synchronization measure $\langle S \rangle$ with further increases in κ. For sufficiently strong coupling $\kappa \gg \sigma_\Delta$, the disruptive effect of disorder on synchronization becomes negligible; however, this regime is beyond the scope of the present study. The onset of chaos stems from the combined influence of stronger coupling and nonzero amplitude-phase coupling α. In the absence of amplitude-phase coupling, the dynamics revert to a

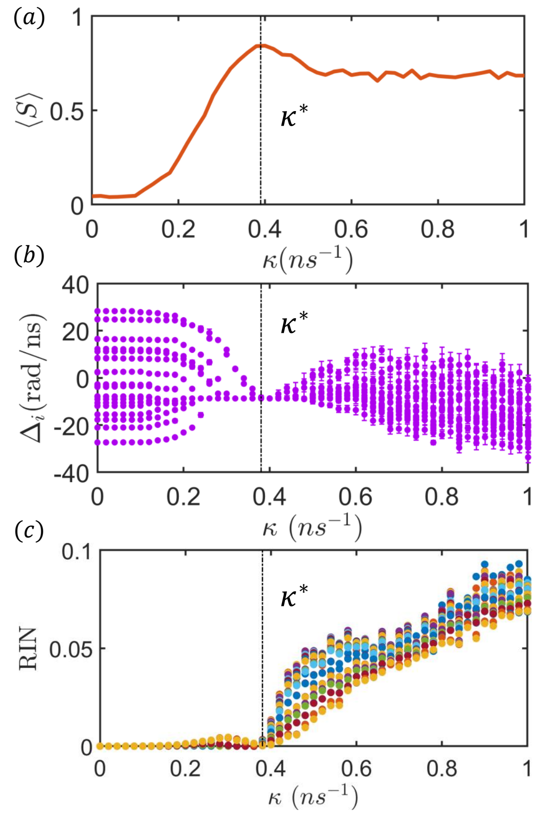

FIG. 2. Optimized steady-state synchronization with fixed frequency disorder in a network of $M = 24$ semiconductor diode lasers. (a) Maximization of synchronization measures $\langle S \rangle$ by an optimal coupling strength κ^*. (b) Average short-term final frequency detuning of the individual lasers versus κ, where the error bars represent the standard deviation calculated over a moving time window of size 3τ with a step size of 0.3τ for $t \in [50, 100]$ns. (c) Mean-square value of the normalized intensity fluctuations, $(I_i(t) - \langle I_i(t) \rangle)/\langle I_i(t) \rangle$, as a function of the coupling parameter κ, serving as a time-domain measure of the relative intensity noise (RIN) of individual lasers over a 50 ns time window. Different colors correspond to different lasers.

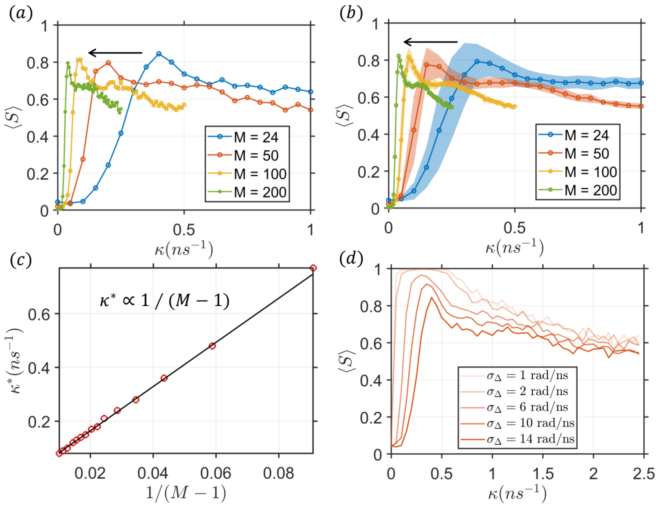

FIG. 3. Robustness and size scaling of optimized steady-state synchronization. The frequency disorders are independently sampled from a Gaussian distribution $\sigma_\Delta \mathcal{N}(0,1)$ with the standard deviation σ_Δ. (a) Optimizing steady-state synchronization for different number M of lasers for $\sigma_\Delta = 14\,\text{rad/ns}$. (b) Statistical fluctuations of the optimized steady-state synchronization, where for each value of M, ten independent realizations of the frequency disorder for $\sigma_\Delta = 14\,\text{rad/ns}$ are tested. The four curves in their respective statistical clouds are the averages and the shaded areas indicate the corresponding standard deviations. (c) Location of the optimized peak, κ^*, indicated by the averaged peak position over ten frequency disorder realizations. The resulting κ^* values exhibit an inverse relationship with the system size: $\kappa^* \propto 1/(M-1)$, demonstrated for $M = [12, 18, 24, 30, 36, 42, 46, 50, 55, 60, 65, 70, 80, 90, 100]$. (d) Effect of frequency disorder strength as characterized by σ_Δ on the steady-state synchronization for $M = 24$. For small values of σ_Δ, the peak value of $\langle S \rangle$ can reach unity as in the corresponding disorder-free system.

steady state at the stronger coupling compared with the weak-coupling regime ($\kappa \ll \sigma_\Delta$) (see SI). Qualitatively, the optimized steady-state synchronization emerges from the interplay among frequency disorder, coupling, and dynamical stability.

Is the optimized steady-state synchronization robust as the laser network becomes larger? Figure 3 provides an affirmative answer. As the network size M increases, the optimal coupling value κ^* decreases, but the optimized steady-state synchronization persists, as shown in Fig. 3(a). This can be understood by noting that the total coupling per laser $\sum_j K_{ij} = \kappa(M-1)$ is assumed to be fixed as in a realistic experimental setting. If approximately the same amount of total coupling per laser is required for the optimized steady-state synchronization to arise, increasing M will naturally result in a reduced κ^* value. As M increases, the statistical variation of the frequency disorder becomes well behaved, leading to narrower fluctuations in the synchronization optimization, as shown in Fig. 3(b). The height of the optimized peak in $\langle S \rangle$ with increasing M remains approximately constant, due to the fact that, at the optimized peak, the total coupling strength per laser remains constant, thereby preserving the steady-state solution and sustaining the same level of synchronization, as explained by our theory below. Quantitatively, the dependence of κ^* on M follows the scaling relation: $\kappa^* \propto 1/(M-1)$, as shown in Fig. 3(c). For $M = 2$ ($M = 24$) coupled lasers, the optimal coupling is $\kappa^* \approx 8\ \text{ns}^{-1}$ ($\kappa^* \approx 0.4\,\text{ns}^{-1}$) [Fig. 3(c)]. The scaling law indicates that increasing the number of lasers significantly reduces the required coupling strength per link (κ^*), whereas the optimal total coupling cost, $\sum_{ij} K^*_{ij} \propto M$, grows linearly with M, consistent with our physical theory presented below. In addition, as the extent of frequency disorder measured by the standard deviation σ_Δ of the frequency distribution is reduced, synchronization is enhanced, as shown in Fig. 3(d).

To explain the optimized steady-state synchronization in Figs. 3(a–d), we develop a physical theory by expanding the LK equations about the steady state, yielding a generalized time-delayed Kuramoto system [50] with an additional phase shift $\tan^{-1}\alpha + \omega_0\tau$ and an effective coupling enhanced by the amplitude–phase coupling $\sqrt{1+\alpha^2}$ [Sec. III in Supplementary Information (SI)]. Introducing the delayed phase differences $\eta_i = \Omega_i(t) - \Omega_i(t-\tau)$, the dynamics can be recast as a gradient flow governed by an effective thermodynamic potential $U(\eta_i)$, which encapsulates the collective coupling influence of the other lasers on laser i. In the absence of frequency disorder ($\Delta_i = \Delta_j = 0$) with all lasers oscillating at the reference frequency ω_0, the coupling configuration $K_{ij} = \kappa(1-\delta_{ij})$ renders the potential identical across the lasers:

$$U(\eta(t)) = \eta^2(t) - 2\tau\sqrt{1+\alpha^2}k^{\text{in}} \cos\left[\eta(t) + \tan^{-1}\alpha + \omega_0\tau\right], \quad (2)$$

where $k^{\text{in}} = \sum_j K_{ij} = \kappa(M-1)$ is the intrinsic coupling strength received by each laser from the others. The local minima of $U(\eta)$ coincide for all lasers at $\eta^* = 2\pi f_{\text{final}}\tau$ that defines the synchronized frequency. The first quadratic term enforces parabolic confinement, while the cosine modulation arises from delay τ, amplitude-phase coupling parameter α, and intrinsic coupling k^{in}. For weak effective coupling $\mathbb{K} \equiv \tau\sqrt{1+\alpha^2}\kappa(M-1) \ll \eta^2$, the modulation is negligible and the system is in a unique synchronized steady state. In contrast, stronger coupling generates multiple local minima leading to multistability that drives the system into chaotic regimes for $\alpha \neq 0$ (see SI).

In the system governed by a smooth quadratic (parabolic) potential without coupling, as indicated by Eq. (2), once the coupling-induced cosine oscillation is excluded, frequency disorder ($\Delta_i \neq \Delta_j$) contributes an additional term $-2\tau\Delta_i\eta_i(t)$ to the thermodynamic potential $U(\eta_i(t))$. As a result, the global minima of the individual lasers become substantially different, hindering synchronization. However, for sufficiently strong coupling, the potential landscape is reshaped by the cosine term in Eq. (2), producing multiple local minima separated by high barriers while leaving the distant global minima unchanged, as shown in Fig. 4(a) for two distinct initial values of detuning Δ_i. For a fixed effective coupling $\mathbb{K}$, the height of the barriers separating the local minima decreases monotonically with increasing η from the global minimum. In the near-overlapping regime, e.g., the red rectangle in Fig. 4(a), the proximity of these local minima leads to nearly synchronized final frequencies. This mechanism enables enhanced frequency and phase locking, even though the system ultimately settles into states that are not global minima.

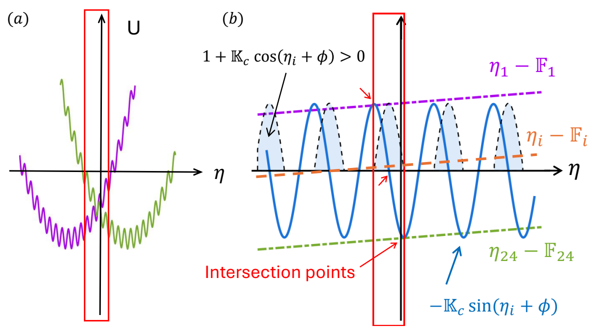

FIG. 4. Schematic of local-minima selection, corresponding to the steady state of each laser. (a) Effective thermodynamic potential comprising a parabolic term, a shifted global minimum $-2\tau\Delta_i\eta_i(t)$, and a coupling-induced cosine component. The red rectangle marks the near-overlapping regime that yields nearly synchronized final frequencies. (b) Illustration of steady-state selection from the local minima of the effective potential landscape for different lasers at the critical effective coupling $\mathbb{K}_c$.

More specifically, the local minima of the potential are determined by the conditions $dU/d\eta_i = 0$ and $d^2U/d\eta_i^2 > 0$, leading to the constraints $\eta_i - \mathbb{F}_i = -\mathbb{K}\sin(\eta_i + \phi)$ and $1 + \mathbb{K}\cos(\eta_i + \phi) > 0$, respectively, where $\mathbb{F}_i \equiv \tau\Delta_i$ denotes the effective detuning and $\phi \equiv \mathrm{mod}(\tan^{-1}\alpha + \omega_0\tau, 2\pi) \approx 0.4\pi$. Given the critical effective coupling $\mathbb{K}_c$, the intersections between the straight lines $\eta_i - \mathbb{F}_i$ and the sinusoidal curves $-\mathbb{K}_c \sin(\eta_i + \phi)$ that satisfy $d^2U/d\eta_i^2 > 0$ define the local minima of the potential, i.e., the steady-state solutions η_i for each laser i, as illustrated in Fig. 4(b). The corresponding local minima η_i determine the final frequencies of the lasers. For small coupling $\mathbb{K} \ll \mathbb{K}_c$, laser frequencies remain widely separated, whereas large coupling $\mathbb{K} \gg \mathbb{K}_c$ induces multistability and chaos via unstable dynamical invariant sets. There exists a critical effective coupling determined by $\mathbb{K}_c = \max(|\mathbb{F}_i|)$, at which all lasers attain their final frequencies within the same regime satisfying $1 + \mathbb{K}\cos(\eta_i + \phi) > 0$, ensuring the local minimum condition $d^2U/d\eta_i^2 > 0$, as highlighted by the red square in Fig. 4(b). In this case, the maximum frequency difference is determined by the width of the regime where $d^2U/d\eta_i^2 > 0$. The onset of such solutions defines the critical effective coupling with the resulting states referred to as near-synchronized steady states. Below this threshold, only a subset of lasers achieve closely aligned final frequencies within the same $1 + \mathbb{K}\cos(\eta + \phi) > 0$ regime.

Beyond this critical effective coupling, the final frequency differences diminish and multiple stable yet distinct near-synchronized steady states emerge. As their stability weakens, synchronization begins to saturate, giving rise to periodic or quasiperiodic phase dynamics. As the coupling strength increases further, the nontrivial amplitude-phase coupling in the LK equation (see SI) can trigger chaos [28, 33], thereby weakening synchronization. The onset of chaos defines the optimized peak at κ^*, as shown in Fig. 2, which typically occurs slightly above the critical coupling strength, as $\kappa^* > \kappa_c$, where κ_c is determined from the critical effective coupling $\mathbb{K}_c$. In contrast, for $\alpha = 0$, the optimized steady-state synchronization in the weak coupling vanishes: synchronized steady states appear only at the stronger coupling, while for weak coupling ($\kappa \ll \sigma_\Delta$) the system is far away from synchronization (see SI).

More specifically, for the frequency disorder $\Delta_i = 14 \times \mathcal{N}(0, 1)$ rad/ns, the maximum effective detuning is $\max(|\mathbb{F}_i|) = \tau|\Delta_0| \approx 90$. To compensate for it, the effective coupling $\mathbb{K}^*$ must exceed $\mathbb{K}_c = \tau|\Delta_0|$, giving $\kappa^* > \kappa_c = |\Delta_0|/[(M-1)\sqrt{1+\alpha^2}] \approx 0.26\,\mathrm{ns}^{-1}$ for $M = 24$, which is consistent with Fig. 3. This relationship reveals the scaling $\kappa^* \propto 1/(M-1)$, thereby explaining the numerical results in Fig.3(c). Moreover, the critical coupling coincides with the necessary condition of the classical Kuramoto model[51–53] in the limit of vanishing amplitude-phase coupling and time delay.

To summarize, we demonstrate that optimal steady-state synchronization can be achieved in the weak-coupling regime of semiconductor diode-laser networks with fixed frequency disorder, and we develop a physical theory that explains both its origin and the associated size-scaling behavior. Remarkably, the peak synchronization level is independent of the number of lasers, while the required coupling cost scales linearly with system size, ensuring robust synchronization even in large arrays. The emergence of this optimal state near the boundary between steady-state and chaotic regimes results from the competition among frequency disorder, coupling effects, and dynamical stability. More broadly, the complex interplay of amplitude and phase dynamics together with time-delay effects makes optimal steady-state synchronization a robust and experimentally observable phenomenon across a wide range of network sizes.

Beyond edge-emitting diode lasers (described by the LK equations), our results can be extended to vertical-cavity surface-emitting lasers and other classes of nonlinear oscillators. In general, variations in intrinsic time constants can influence the onset of chaotic behavior and thereby modify the optimal coupling strength. Overall, the present findings extend beyond the traditional Kuramoto paradigm and establish semiconductor laser networks as a promising platform for investigating disorder-enhanced collective dynamics.

This work was supported by the Office of Naval Research under Grant No. N00014-24-1-2548.

---

[1] Y. Kuramoto, *Chemical Oscillations, Waves, and Turbulence* (Springer, Berlin, 1984).

[2] A. Pikovsky, M. Rosenblum, and J. Kurths, *Synchronization: A Universal Concept in Nonlinear Science* (Cambridge University Press, Cambridge, 2003).

[3] L. M. Pecora and T. L. Carroll, Master stability functions for synchronized coupled systems, Phys. Rev. Lett. **80**, 2109 (1998).

[4] L. Huang, Q. Chen, Y.-C. Lai, and L. M. Pecora, Generic behavior of master-stability functions in coupled nonlinear dynamical systems, Phys. Rev. E **80**, 036204 (2009).

[5] L. M. Pecora, T. L. Carroll, G. A. Johnson, D. J. Mar, and J. F. Heagy, Fundamentals of synchronization in chaotic systems, concepts, and applications, Chaos **7**, 520 (1997).

[6] S. Watanabe and S. H. Strogatz, Integrability of a globally coupled oscillator array, Phys. Rev. Lett. **70**, 2391 (1993).

[7] E. Ott and T. M. Antonsen, Low dimensional behavior of large systems of globally coupled oscillators, Chaos **18**, 037113 (2008).

[8] G. Mikaberidze and D. Taylor, Emergent topology of optimal networks for synchrony, arXiv preprint arXiv:2509.18279 (2025).

[9] C. R. S. Williams, T. E. Murphy, R. Roy, F. Sorrentino, T. Dahms, and E. Schöll, Experimental observations of group synchrony in a system of chaotic optoelectronic oscillators, Phys. Rev. Lett. **110**, 064104 (2013).

[10] C. Williams, F. Sorrentino, T. E. Murphy, and R. Roy, Synchronization states and multistability in a ring of periodic oscillators: Experimentally variable coupling delays, Chaos **23**, 143117 (2013).

[11] J. D. Hart, J. P. Pade, T. Pereira, T. E. Murphy, and R. Roy, Adding connections can hinder network synchronization of time-delayed oscillators, Phys. Rev. E **92**, 022804 (2015).

[12] Y. C. Ji, I. Uzelac, N. Otani, S. Luther, R. F. J. Gilmour, E. Cherry, and F. Fenton, Synchronization as a mechanism for low-energy anti-fibrillation pacing, Heart Rhyt. **14**, 1254 (2017).

[13] Y. Tang, F. Qian, H. Gao, and J. Kurths, Synchronization in complex networks and its application–a survey of recent advances and challenges, Annu. Rev. Control **38**, 184 (2014).

[14] S. Boccaletti, A. N. Pisarchik, C. I. Del Genio, and A. Amann, *Synchronization: from coupled systems to complex networks* (Cambridge University Press, 2018).

[15] S. F. Brandt, B. K. Dellen, and R. Wessel, Synchronization from disordered driving forces in arrays of coupled oscillators, Phys. Rev. Lett. **96**, 034104 (2006).

[16] Y. Zhang and A. E. Motter, Identical synchronization of nonidentical oscillators: when only birds of different feathers flock together, Nonlinearity **31**, R1 (2018).

[17] Y. Zhang, J. L. Ocampo-Espindola, I. Z. Kiss, and A. E. Motter, Random heterogeneity outperforms design in network synchronization, Proc. Natl. Acad. Sci. (USA) **118**, e2024299118 (2021).

[18] Y. Zhang, Y. Sugitani, and A. E. Motter, Synchronizing chaos with imperfections, Phys. Rev. Lett. **126**, 164101 (2021).

[19] A. Nazerian, S. Panahi, and F. Sorrentino, Synchronization in networked systems with large parameter heterogeneity, Commun. Phys. **6**, 253 (2023).

[20] A. Argyris, M. Bourmpos, and D. Syvridis, Experimental synchrony of semiconductor lasers in coupled networks, Opt. Express **24**, 5600 (2016).

[21] B. Kim, N. Li, A. Locquet, and D. Citrin, Experimental bifurcation-cascade diagram of an external-cavity semiconductor laser, Opt. Express **22**, 2348 (2014).

[22] N. Nair, K. Hu, M. Berrill, K. Wiesenfeld, and Y. Braiman, Using disorder to overcome disorder: A mechanism for frequency and phase synchronization of diode laser arrays, Phys. Rev. Lett. **127**, 173901 (2021).

[23] O. Spitz, S. Koyu, P. Nyaupane, M. Berrill, and Y. Braiman, Complex spatio-temporal non-linear dynamics in a 1d-array of 23 broad-area semiconductor laser diodes under external optical feedback, in *Laser Technology for Defense and Security XVIII*, Vol. 12515 (SPIE, 2023) pp. 14–21.

[24] S. Koyu, O. Spitz, M. A. Berrill, and Y. Braiman, Dynamics and phase-locking in large heterogeneous arrays of semiconductor diode lasers, in *High-Power Diode Laser Technology XXI*, Vol. 12403 (SPIE, 2023) pp. 199–215.

[25] L. Zhang, W. Pan, L. Yan, B. Luo, X. Zou, and S. Li, Isochronous synchronization induced by topological heterogeneity in semiconductor laser networks, Opt. Laser Technol. **153**, 108243 (2022).

[26] J. Tiana-Alsina and C. Masoller, Dynamics of a semiconductor laser with feedback and modulation: Experiments and model comparison, Opt. Express **30**, 9441 (2022).

[27] T. Niiyama and S. Sunada, Power-law fluctuations near critical point in semiconductor lasers with delayed feedback, Phys. Rev. Res. **4**, 043205 (2022).

[28] H. G. Winful and L. Rahman, Synchronized chaos and spatiotemporal chaos in arrays of coupled lasers, Phys. Rev. Lett. **65**, 1575 (1990).

[29] P. Alsing, V. Kovanis, A. Gavrielides, and T. Erneux, Lang and kobayashi phase equation, Phys. Rev. A **53**, 4429 (1996).

[30] D. Lenstra, Statistical theory of the multistable external-feedback laser, Opt. Commun. **81**, 209 (1991).

[31] R. L. Davidchack, Y.-C. Lai, A. Gavrielides, and V. Kovanis, Chaotic transitions and low-frequency fluctuations in semiconductor lasers with optical feedback, Physica D: Nonlinear Phenom. **145**, 130 (2000).

[32] R. Lang and K. Kobayashi, External optical feedback effects on semiconductor injection laser properties, IEEE J. Quantum Electron. **16**, 347 (1980).

[33] H. G. Winful and S. S. Wang, Stability of phase locking in coupled semiconductor laser arrays, Appl. Phys. Lett. **53**, 1894 (1988).

[34] A. E. D. Barioni, A. N. Montanari, and A. E. Motter, Interpretable disorder-promoted synchronization and coherence in coupled laser networks, Phys. Rev. Lett. **135**, 197401 (2025).

[35] L.-L. Ye, N. Vigne, F.-Y. Lin, H. Cao, and Y.-C. Lai,

Optimal sparse networks for synchronization of semiconductor lasers, arXiv preprint arXiv:2511.03205 (2025).

[36] P. Mu, Y. Huang, P. Zhou, Y. Zeng, Q. Fang, R. Lan, P. He, X. Liu, G. Guo, X. Liu, *et al.*, Extreme events in two laterally-coupled semiconductor lasers, Opt. Express **30**, 29435 (2022).

[37] R. Zhang, S. Yang, Y. Han, Y. Lu, T. Wu, Z. Tang, D. Liu, S. Zheng, and M. Zhang, Single transverse-mode and single longitudinal-mode parity-time symmetric fabry-perot laser array, Opt. Express **32**, 47647 (2024).

[38] A. Argyris, D. Syvridis, L. Larger, V. Annovazzi-Lodi, P. Colet, I. Fischer, J. García-Ojalvo, C. R. Mirasso, L. Pesquera, and K. A. Shore, Chaos-based communications at high bit rates using commercial fibre-optic links, Nature **438**, 343 (2005).

[39] A. Uchida, F. Rogister, J. García-Ojalvo, and R. Roy, Synchronization and communication with chaotic laser systems, Prog. Opt. **48**, 203 (2005).

[40] A. Uchida, K. Amano, M. Inoue, K. Hirano, S. Naito, H. Someya, I. Oowada, T. Kurashige, M. Shiki, S. Yoshimori, K. Yoshimura, and P. Davis, Fast physical random bit generation with chaotic semiconductor lasers, Nat. Photon. **2**, 728 (2008).

[41] F.-Y. Lin and J.-M. Liu, Chaotic lidar, IEEE J. Sel. Top. Quan. Elec. **10**, 991 (2004).

[42] F.-Y. Lin and J.-M. Liu, Chaotic radar using nonlinear laser dynamics, IEEE J. Quan. Elec. **40**, 815 (2004).

[43] C.-H. Cheng, C.-Y. Chen, J.-D. Chen, D.-K. Pan, K.-T. Ting, and F.-Y. Lin, 3D pulsed chaos lidar system, Opt. Express **26**, 12230 (2018).

[44] D. Brunner and I. Fischer, Reconfigurable semiconductor laser networks based on diffractive coupling, Opt. Lett. **40**, 3854 (2015).

[45] D. Botez, L. Mawst, P. Hayashida, G. Peterson, and T. J. Roth, High-power, diffraction-limited-beam operation from phase-locked diode-laser arrays of closely spaced "leaky" waveguides (antiguides), Appl. Phys. Lett. **53**, 464–466 (1988).

[46] G. Kozyreff, A. G. Vladimirov, and P. Mandel, Global coupling with time delay in an array of semiconductor lasers, Phys. Rev. Lett. **85**, 3809 (2000).

[47] A. Argyris, M. Bourmpos, and D. Syvridis, Experimental synchrony of semiconductor lasers in coupled networks, Opt. Express **24**, 5600 (2016).

[48] N. Nair, E. Bochove, and Y. Braiman, Almost perfect in-phase and anti-phase chaotic and periodic phase synchronization in large arrays of diode lasers, Opt. Commun. **430**, 104 (2019).

[49] N. Nair, E. Bochove, and Y. Braiman, Phase-locking of arrays of weakly coupled semiconductor lasers, Opt. Exp. **26**, 20040 (2018).

[50] M. S. Yeung and S. H. Strogatz, Time delay in the kuramoto model of coupled oscillators, Phys. Rev. Lett. **82**, 648 (1999).

[51] N. Chopra and M. W. Spong, On exponential synchronization of Kuramoto oscillators, IEEE Trans. Autom. Control **54**, 353 (2009).

[52] A. Jadbabaie, N. Motee, and M. Barahona, On the stability of the Kuramoto model of coupled nonlinear oscillators, in *Proc. Amer. Control Conf. (ACC), 2004*, Vol. 5 (IEEE, 2004) pp. 4296–4301.

[53] F. Dörfler and F. Bullo, On the critical coupling for kuramoto oscillators, SIAM J. Appl. Dyn. Syst. **10**, 1070 (2011).